Journal of Molecular Structure 1038 (2013) 220–229

Contents lists available at SciVerse ScienceDirect

Journal of Molecular Structure

journal homepage: www.elsevier.com/locate/molstruc

Characterization of acetylacetonato carbonyl diphenyl-2-pyridylphosphine rhodium(I): Comparison with other carbonyl complexes

Walter Purcell *, Jeanet Conradie *, Trevor T. Chiweshe, Johan A. Venter, Hendrik G. Visser, Michael P. Coetzee

Department of Chemistry, University of the Free State, 205 Nelson Mandela Drive, Bloemfontein 9300, South Africa

HIGHLIGHTS

- Rh(I)/Rh(III) complexes exhibit n(CO) stretching frequencies in narrow IR range.
- Two independent [Rh(acac)(CO)(DPP)] molecules exit due to the difference in pyridyl ring orientations.
- DFT calculations indicate 12 areas of minimum energy for the DPP orientation in [Rh(acac)(CO)(DPP)].
- DFT calculations corroborate the crystal structure observations.

ARTICLE INFO

Article history:
Received 22 October 2012
Received in revised form 22 January 2013
Accepted 24 January 2013
Available online 1 February 2013

Keywords:
Rhodium(I)
Diphenyl-2-pyridylphosphine
Carbonyl
Oxidative addition
Methyl iodide
Donor ligands

ABSTRACT

Different rhodium(I)/(III) diphenyl-2-pyridylphosphine complexes were isolated and successfully characterized. The [Rh(acac)(CO)(DPP)] (DPP = diphenyl-2-pyridylphosphine) complex crystallizes in the $P\bar{1}$ space group with four molecules per unit cell. The results clearly show that the differences between the two independent molecules are mainly centered around the orientation of the pyridyl ring within the two square planer molecules. The results also indicate that the phosphine ligands act as monodentate ligands in both molecules, with Rh–P and Rh–CO bond distances of 2.243(1); 2.235(1) and 1.791(4); 1.776(4) Å respectively. A comparison of the ν(CO) stretching frequencies of a relatively large number of rhodium complexes indicated little overlap between the ν(CO) of different types of complexes (e.g. Rh(I) vs Rh(III)) and relatively small standard deviations within each type of complex. DFT calculations were used to determine the preferred pyridyl ring orientation. These calculations indicated that at least 12 areas of minimum energy, which exists as broad, low energy wells, are theoretically suitable for DPP group orientation within this kind of structure.

1. Introduction

Organometallic complexes of rhodium have attracted a lot of attention in the last few decades, mainly due to the metal's scope and versatility as homogeneous and heterogeneous catalysts in a large variety of industrial processes [1–4]. These processes include the production of acetic acid via the Monsanto process [5,6] and the commercial production of L-dopa [7] for the treatment of Parkinson's disease. Recent interest in the metal was mainly driven by the discovery that complexes such as $Rh_2(\mu\text{-}O_2CCF_3)_4$ [8] and $Rh_2(\mu\text{-}HNCOCF_3)_4$ [9] exhibit carcinostatic activity. Developing new, more effective catalysts depend on the understanding of the mechanism of action of rhodium complexes in existing catalytic processes. The key to research on these kinds of catalytic processes and cycles is the greater understanding of the relationships between activity and catalyst structure, as well as ways to better predict, understand and control catalyst molecular architecture.

The conversion of methanol to acetic acid such as in the Monsanto process using $[Rh(CO)_2I_2]^-$ as catalyst [10] involves six different steps, including oxidative addition, 1,1-insertion or CO insertion, CO association and reductive elimination. A group of [Rh(LL)(CO)(BX_3)] complexes (LL = mono ionic bidentate ligands and BX_3 = different phosphines, phosphites, arsines and stibines) came to our attention as possible candidates for catalysis or model complexes. The ability of these complexes to undergo oxidative addition at relatively mild conditions as well as the possibility to change the steric bulk and electronic properties of the complexes with ease, made them ideal candidates to investigate the effect of these changes on the rate of oxidative addition reactions. Numerous structural and kinetic studies [11] were undertaken to elucidate mechanistically the influences of factors such as

* Corresponding authors. Tel.: +27 (0)514012200; fax: +27 (0)865255382.
E-mail addresses: purcellw@ufs.ac.za (W. Purcell), conradj@ufs.ac.za (J. Conradie).

0022-2860/$ - see front matter © 2013 Published by Elsevier B.V.
http://dx.doi.org/10.1016/j.molstruc.2013.01.061

Table 1
Carbonyl stretching frequencies for different rhodium complexes.

Complex	LL	PX_3	ν(CO) (cm^{-1})	Refs.
$[Rh(LL)(CO)_2]$	acac		2063, 1998	[24,25]
	cupf		2087, 2013	[26]
	Ox		2065, 1992	[27]
	Sox		2080, 2005	[27]
	tmhd		2074, 2002	[28]
	dbm		2080, 1998	[11,28]
	btfac		2088, 2024	[29]
	tfac		2086, 2026	[11,28]
	hfac		2082, 2008	[11,28]
	fctfa		2074, 2008	[30]
	fca		2068, 2014	[30]
	bfcm		2074, 1998	[30]
	dfcm		2074, 2008	[30]
	bap		2065, 2008	[31]
	bab		2084, 2014	[36]
$[Rh(LL)(CO)(PX_3)]$	acac	PPh_3	1986	[24,25]
		$P(p\text{-}ClC_6H_4)_3$	1980	[32]
		$P(p\text{-}Tol)_3$	1980	[11,28]
		$P(p\text{-}MeOC_6H_4)_3$	1972	[32]
		DPP	1975	[15,33]
	cupf	PCy_3	1989	[26,32]
		PPh_3	1982	[26,32]
		DPP	1981	[33]
		$P(Ph_2C_6H_4)_3$	1978	[26,32]
		$P(p\text{-}ClC_6H_4)_3$	1971	[26,32]
		$P(p\text{-}MeOC_6H_4)_3$	1965	[26,32]
		$P(p\text{-}Tol)_3$	1965	[26,32]
	tmhd	$P(p\text{-}Tol)_3$	1980	[28]
	dbm	$P(p\text{-}Tol)_3$	1983	[11,28]
	btfac	$P(p\text{-}Tol)_3$	1986	[29]
	tfac	$P(p\text{-}Tol)_3$	1983	[11,28]
	hfac	$P(p\text{-}Tol)_3$	1998	[11,28]
	btfac	PPh_3	1984	[29]
	neocupf	PPh_3	1976	[32]
	sacac	PPh_3	1978	[11]
	dmavk	PPh_3	1960	[37]
		$P(p\text{-}ClC_6H_4)_3$	1960	[32]
	tavk	PPh_3	1974	[34]
		$P(p\text{-}MeOC_6H_4)_3$	1960	[34]
	fctfa	PPh_3	1986	[30]
	fca	PPh_3	1980	[30]
	bfcm	PPh_3	1977	[30]
	dfcm	PPh_3	1977	[30]
	tta	PPh_3	1981	[35]
	bap	PPh_3	1982	[36]
	bab	PPh_3	1981	[36]
$[Rh(LL)(CO)(PX_3)(CH_3)I]$	acac	PPh_3	2060	[11]
		$P(p\text{-}ClC_6H_4)_3$	2064	[32]
		$P(p\text{-}MeOC_6H_4)_3$	2056	[32]
		DPP	2048	[15,33]
	cupf	DPP	2061	[15,33]
		PPh_3	2052	[26,32]
		$P(p\text{-}ClC_6H_4)_3$	2052	[26,32]
		PCy_3	2049	[26,32]
		$P(p\text{-}MeOC_6H_4)_3$	2045	[26,32]
	neocupf	PPh_3	2048	[32]
	dmavk	PPh_3	2070	[37]
	fctfa	PPh_3	2056	[30]
$[Rh(LL)(COCH_3)(PX_3)I]$[b]	acac	DPP	1721	[15,33]
	cupf	DPP	1692	[33]
	dmavk	PPh_3	1716	[37]
	macsm	PPh_3	1712	[38]
	stsc	PCy_3	1710	[38]
	cupf	$P(OCH_2)_3CCH_3$	1704	[32]
$[Rh(LL)(COCH_3)(NSO_2)(PPh_3)]$[b]	macsm	PMe_2Ph	1716	[39]
$[Rh(LL)_3(COCH_3)(Cl)]^+$[b]	PMe_2Ph	–	1720	[40]
$[Rh(LL)(COCH_3)I_2]$[b]	dppm	–	1709	[41]
$[Rh(LLl)(COCH_3)I_2]$[b]	dppmo	–	1704	[42]
$[Rh(LL)(COCH_3)I_2]$[b]	dppms	–	1701	[42]
$[Rh(LL)(COCH_3)I_2]$[b]	dppe	–	1713	[41]
$[Rh(LL)(COCH_3)I_2]$[b]	dppp	–	1698	[43]

Hacac = 2,4-pentanedione (acetylacetone); Hba = 1-phenyl-1,3-butanedione; Hbfcm = 1-ferrocenyl-3-phenylpropane-1,3-dione; Hdbm = 1,3-diphenyl-1,3-propanedione; Hdfcm = 1,3-diferrocenylpropane-1,3-dione; Hfca = 1-ferrocenylbutane-1,3-dione; Hfctca = 1-ferrocenyl-4,4,4-trichlorobutane-1,3-dione; Hfctfa = 1-ferrocenyl-4,4,4-trifluorobutane-1,3-dione; Hhfac = 1,1,1,5,5,5-hexafluoro-2,4-pentanedione; Htfa = 1,1,1-trifluoro-2,4-pentanedione; Hbtfb = 1,1,1-trifluoro-4-phenyl-2,4-butanedione, Htmdh = tetramethylheptanedione, trifluorobenzoylacetone; Htta = thenoyltrifluoroacetone; Hbap = 1-phenylpentane-1,3-dione; Hbab = 1-phenylhexane-1,3-dione; Hneocupf = N-nitroso-N-naphthylhydroxylamine; Hsacac = thioacetylacetone; Hdmavk = dimethylaminovinylketone; Hmacsm = methyl(2-methyl-amino-1-cyclopentene-1-dithiocarboxylate); Hstsc = salicylaldehydethiosemicarbazose; Htavk = 2-aminovinyl-5,5,5-trifluoro 4 pentanone; Hcupf = N-hydroxy-N-nitrosobenzeneamine; HOx = 8-hydroxyquinoline; HSox = salicylaldoxide; Hdmh = dibenzoylmethane dppm = $Ph_2PCH_2PPh_2$; dppmo = $Ph_2PCH_2P(O)Ph_2$; dppms = $Ph_2PCH_2P(S)Ph_2$; dppe = $Ph_2PCH_2CH_2PPh_2$; and dppp = $Ph_2P(CH_2)_3PPh_2$.

[b] $\nu(COCH_3)$.

nucleophilicity of the metal centers, solvent interactions and steric bulk on the rate of oxidative addition and CO insertion.

Recently diphenyl-2-pyridylphosphine (DPP) [12] came to our attention as ligand due to its ability to not only coordinate to the metal ion with the phosphorus atom [13], but also with the pyridyl nitrogen making the phosphine ligand a potential bidentate ligand [14]. The increase in electron density due to the presence of a nitrogen atom in the phosphine also has the potential to alter the Lewis basicity of the phosphine and ultimately influence the oxidative addition reactions for the metal complexes. With this in mind we prepared and structurally characterized [Rh(acac)(CO)(DPP)] [15] to investigate the phosphine's mode of bonding as well as possible oxidative addition products for the reaction between methyl iodide and the mono carbonyl complex.

2. Experimental

2.1. General considerations

All chemicals used in the syntheses were of reagent grade and were used without further purification. The $RhCl_3{\cdot}3H_2O$ and diphenyl-2-pyridylphosphine were purchased from Sigma–Aldrich. Solvents were purified and dried prior to use by standard procedures. ^1H and ^{31}P NMR spectra were measured on a Bruker AVANCE DPX 300 MHz spectrometer and the ^{13}C NMR spectra on a Bruker AVANCE II 600 MHz spectrometer. ^1H NMR and proton decoupled ^{13}C NMR data are listed in the order: chemical shift (δ, reported in ppm and referenced to TMS), integral value, multiplicity, coupling constant (J, in Hz) and assignment. Proton decoupled ^{31}P NMR data are listed in the order: chemical shift (δ), multiplicity and coupling constant (J, in Hz). For the characterization of the

Rh(III) alkyl and acyl species [Rh(acac)(CO)(DPP)] (5 mg, 0.0101 mmol) was dissolved in 0.7 ml $CDCl_3$ and transferred to a 5 mm diameter NMR tube. Methyl iodide (6.31 μl, 0.101 mmol) was added and ^1H and ^{31}P NMR spectra recorded every 0.5 h. The CHN analysis was performed on a LECO Truspec micro-analyzer.

A Shimadzu ICPS-7510 ICP-OES with a radial-sequential plasma spectrometer was used for the wet chemical analysis of all the rhodium samples in the current study [16]. The torch of the ICP-OES was mounted vertically with the plasma being viewed in the radial, instead of the axial, mode due to the better detection limits achieved with this configuration. The rhodium content in all of the rhodium compounds was analyzed using a cobalt internal standard method at an atomic wavelength for rhodium of 343.489 nm and ionic wavelength for cobalt of 228.616 nm [16]. The rhodium standard (1000 ppm) was purchased from Aldrich Chemicals while the analytical grade HCl (32%), HNO_3 (65%) and $Co(NO_3)_2{\cdot}6H_2O$ were obtained from Merck Chemicals. Dilution of the solutions was done using double distilled water and Schott Duran grade (A) type glassware was used for all chemical analysis.

Intensity data was collected at −100 °C on a Bruker APEX(II) CCD area detector diffractometer with graphite monochromated Mo Kα radiation (50 kV, 30 mA). The data was collected with ϕ and ϖ-scans at 0.5° width while data reduction was performed with SAINT+ [17]. The crystal structure was solved by direct methods using SHELXTL [18]. Non-hydrogen atoms were first refined by full matrix least-squares calculations based on F^2 using SHELXTL. Hydrogen atoms were first located in the difference map, then positioned geometrically and allowed to ride on their respective parent atoms. Diagrams and publication material were generated using SHELXTL and PLATON [19].

2.2. Synthesis

2.2.1. [Rh(acac)(CO)$_2$]

[Rh(acac)$(CO)_2$] was synthesized as previously reported [20]. Yield: 69% IR data (solid state): ν(CO) = 2063, 1998 cm^{-1}. Elemental *Anal.* $RhO_4C_7H_7$: (calculated values in brackets): C, 32.41 (32.58), H, 2.85 (2.74), Rh, 39.68 (39.88)%. ^1H NMR (300 MHz, $CDCl_3$, 20 °C): δ 5.63 (s, CH-acac), 2.09 (s, CH_3-acac), $^{13}C\{^1H\}$ NMR (151 MHz, $CDCl_3$, 20 °C): δ 187.2 (s, C-acac), 183.6 (d, $^1J_{Rh-C}$ = 72.9 Hz, 2 × CO), 101.6 (s, CH-acac), 27.0 (s, 2 × CH_3-acac).

2.2.2. [Rh(acac)(CO)(DPP)]

[Rh(acac)$(CO)_2$] (0.2 g, 0.78 mmol) was dissolved in 10 ml methanol and the solution was slightly heated to 30 °C for 5 min to ensure homogeneity. Diphenyl-2-pyridylphosphine (0.2 g, 0.76 mmol) was added gently whilst stirring and the solution changed color from yellow to red and a yellow product precipitated immediately from the solution. The precipitate was removed by filtration, washed with methanol and dried in a fume cupboard. [Rh(acac)(CO)(DPP)] (0.109 g, 0.22 mmol) was dissolved in 5 ml chloroform and left to stand for 24 h. Yellow crystals suitable for X-ray structure determination were isolated. Yield: 29%. IR data (solid state): ν(CO) = 1975 cm^{-1}. Elemental *Anal.* $RhC_{23}H_{21}NO_3P$, (calculated values in brackets): C, 54.74 (55.14), H, 4.30 (4.30), N, 2.45 (2.84), Rh, 20.54 (20.86). ^1H NMR (300 MHz, $CDCl_3$, 20 °C): δ 8.70 (1H, dd, $^3J_{H-H}$ = 4.6 Hz, $^4J_{H-H}$ = 2.1 Hz, 3-H pyridyl-ring), 7.95 (1H, m, $^3J_{H-H}$ = 7.7 Hz, $^3J_{H-H}$ = 6.0 Hz, $^4J_{H-H}$ = 2.1 Hz, 5-H pyridyl-ring), 7.74 (4H, m, 3- & 5-H phenyl), 7.62 (1H, m, $^3J_{H-H}$ = 7.7 Hz, $^4J_{H-H}$ = 1.7 Hz, 6-H pyridyl-ring), 7.45–7.15 (7H, 4-H pyridyl-ring, 2- & 6-H phenyl, 4-H phenyl), 5.35 (1H, s, CH-acac), 2.02 (3H, s, CH_3-acac), 1.45 (3H, s, CH_3-acac), $^{13}C\{^1H\}$ NMR (151 MHz, $CDCl_3$, 20 °C): δ 187.79 (dd, $^1J_{Rh-C}$ = 75.9 Hz, $^2J_{P-C}$ = 24.2 Hz, CO), 187.44 (s, C-acac), 185.37 (s, C-acac), 157.54 (d, $^1J_{P-C}$ = 71.0 Hz, 1-C pyridyl-ring), 149.95 (d, $^3J_{P-C}$ = 14.3 Hz, 3-C pyridyl-ring), 135.43 (d, $^3J_{P-C}$ = 9.4 Hz, 5-C pyridyl-ring), 134.86 (d, $^2J_{P-C}$ = 11.6 Hz, 2- & 6-C phenyl), 132.15 (d, $^2J_{P-C}$ = 51.6 Hz, 6-C pyridyl-ring), 131.16 (d, $^1J_{P-C}$ = 26.7 Hz, 1-C phenyl), 130.33 (d, $^4J_{P-C}$ = 2.2 Hz, 4-C phenyl), 127.93 (d, $^3J_{P-C}$ = 10.7 Hz, 3- & 5-C phenyl), 123.78 (d, $^4J_{P-C}$ = 2.1 Hz, 4-C pyridyl-ring), 100.67 (s, CH-acac), 27.55 (s, CH_3-acac), 26.58 (s, CH_3-acac), $^{31}P\{^1H\}$ NMR (121 MHz, $CDCl_3$, 20 °C): δ 50.41 (d, $^1J_{Rh-P}$ = 176.0 Hz).

2.2.3. [Rh(acac)(CO)(DPP)(CH_3)I]

Methyl iodide (0.64 g, 4.55 mmol) was added to a well stirred solution containing [Rh(acac)(CO)(DPP)] (0.25 g, 0.46 mmol) in 5 ml chloroform. The reaction was allowed to proceed for 20 min at room temperature during which the color changed from orange to red brown. The solvent was removed by evaporation to yield the final powdered brown product. Yield: 60%. IR data (solid state): ν(CO) = 2048 cm^{-1}. Elemental *Anal.* $RhC_{24}H_{24}INO_3P$ (calculated values in brackets): C, 45.68 (45.37), H, 3.47 (3.92), N, 1.90 (2.21), Rh, 16.95 (16.20). ^1H NMR (300 MHz, $CDCl_3$, 20 °C): δ 8.79 (1H, dd, $^3J_{H-H}$ = 4.6 Hz, $^4J_{H-H}$ = 2.1 Hz, 3-H pyridyl-ring), 8.06 (2H, m, 3- or 5-H phenyl), 7.66 (2H, m, 3- or 5-H phenyl), 7.55 (1H, m, $^3J_{H-H}$ = 7.7 Hz, $^4J_{H-H}$ = 3.5 Hz, 6-H pyridyl-ring), 7.50–7.15 (8H, 4- & 5-H pyridyl-ring, 2- & 6-H phenyl, 4-H phenyl), 5.39 (1H, s, CH-acac), 1.99 (3H, s, CH_3-acac), 1.81 (3H, s, CH_3-acac), 1.21 (3H, dd, $^2J_{Rh-H}$ = 2.0 Hz, $^3J_{P-H}$ = 2.0 Hz, Rh–CH_3), $^{31}P\{^1H\}$ NMR (121 MHz, $CDCl_3$, 20 °C): δ 39.09 (d, $^1J_{Rh-P}$ = 128.4 Hz).

2.2.4. [Rh(acac)($COCH_3$)(DPP)I]

Methyl iodide (0.76 g, 4.55 mmol) was added to a well stirred solution containing [Rh(acac)(CO)(DPP)] (0.19 g, 0.44 mmol) in 5 ml chloroform. The reaction was allowed to proceed for 200 min. at room temperature during which the color changed from orange to red brown. The solution was removed by evaporation to yield the red brown powdered product. Yield: 80%. IR data (solid state): ν(COCH3) = 1721 cm^{-1}. Elemental *Anal.* $RhC_{24}H_{24}INO_3P$ (calculated values in brackets): C, 45.38 (45.37), H, 3.98 (3.82), N, 2.90 (2.21), Rh, 16.15 (16.20). $^{31}P\{^1H\}$ NMR (121 MHz, $CDCl_3$, 20 °C): δ 27.2 (d, $^1J_{Rh-P}$ = 150.9 Hz).

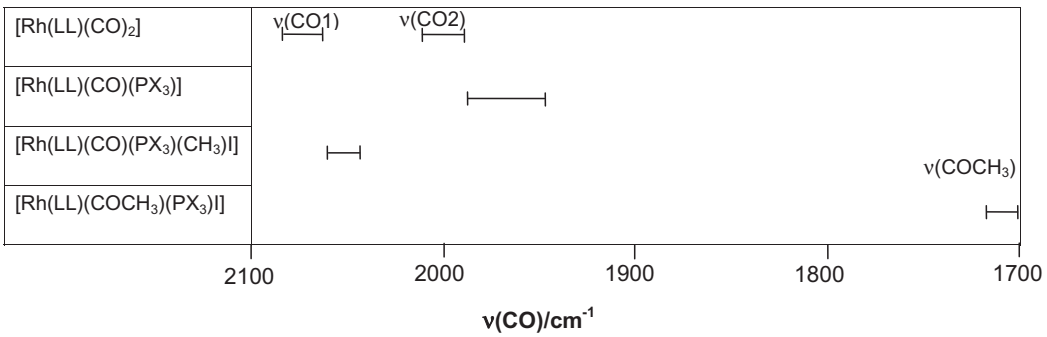

Fig. 1. Carbonyl stretching frequencies in rhodium complexes.

2.3. Computational chemistry

Density functional theory (DFT) calculations were carried out using the ADF (Amsterdam Density Functional) programme [21] with the GGA (Generalized Gradient Approximation) functional PW91 (Perdew-Wang, 1991) [22]. The TZP (Triple ζ polarized) basis set, with a fine mesh for numerical integration, a spin-restricted formalism and full geometry optimization with tight convergence criteria, was used.

3. Results

3.1. Synthesis

The elemental analyses and different NMR results clearly indicate the successful preparation and characterization of the different rhodium DPP carbonyl complexes in normal atmospheric conditions. The synthesis and isolation of the target compounds under these less demanding experimental conditions (Schlenk techniques and inert atmosphere [12]) and in different solvents illustrate the ease of synthesis of these type of complexes. Characterization of the products using IR indicates that the following consecutive reactions took place:

$$[Rh(acac)(CO)_2] \overset{+DPP}{\underset{-CO}{\rightarrow}} [Rh(acac)(CO)(DPP)] \overset{+CH_3I}{\leftrightarrows} [\underset{Rh(III)}{Rh}(acac)(\underset{alkyl}{CO})(DPP)(CH3)(I)] \quad (1)$$

$$[\underset{Rh(III)}{Rh}(acac)(\underset{alkyl}{CO})(DPP)(CH_3)(I)] \leftrightarrows [\underset{Rh(III)}{Rh}(acac)(DPP)(\underset{acyl}{COCH_3})(I)] \quad (2)$$

The dicarbonyl complex $[Rh(acac)(CO)_2]$ clearly show two distinctive carbonyl peaks at 2063 and 1998 cm^{-1} which changes to one peak with ν(CO) at 1975 cm^{-1} after the addition of DPP due to the subsequent substitution of one of the carbonyl ligands and compares favorably with the 1981 cm^{-1} (KBr) that was obtained for the same complexes that was reported by Wajda-Hermanowicz [12]. This shift in ν(CO) is in accordance with previous studies which indicate an increase in electron density on the metal center which can be attributed to the electronegativity of the phosphine and the absence of competition by the other carbonyl ligand. The addition of CH_3I results in the oxidation of Rh(I) to Rh(III) with the simultaneous addition of CH_3 and I to the metal center as illustrated by the ν(CO) shift to 2048 cm^{-1}. The spontaneous CO insertion reaction resulted in the appearance of the $\nu(COCH_3)$ at 1721 cm^{-1}. The decrease in ν(CO) indicated an increase in the metal–carbon π-back-bonding and a decrease in carbon–oxygen triple bond character.

A comparison of the IR data for the monodentate carbonyl complexes obtained in this study and those for previously synthesized complexes revealed very interesting results. In the case of the Rh-acac complexes the ν(CO) for the DPP ligand appeared to be on the lower end of the ν(CO) scale for both the mono carbonyl and alkyl product if it was compared to the different phosphines studied to date (see Table 1). This could easily be explained by the presence of the pyridine ring in DPP. The additional electron density present in the phosphine as a result of the nitrogen increased the electron density on the Rh center resulting in an increase in π-back donation to the carbonyl carbon, thus increasing synergistic σ-back-donation to the metal and subsequently lowering the ν(CO) (weaker carbon oxygen bond). This situation changed however for the corresponding cupf complex. The results in Table 1 clearly showed that the ν(CO) for the cupferrate ligand was approximately the same as for triphenylphosphine and in the same order as all the other phosphine ligands listed.

Close inspection of the reported ν(CO) for this relatively large group of rhodium complexes, obtained from different solvents as well as KBr, indicated that almost no carbonyl stretching frequency overlapping occurred between any of the different types of complexes indicated in Fig. 1. Also important from these results is that neither the solvent nor the solid state plays a very important role in the position of the ν(CO) for the different type of complexes. The limits for ν(CO1) and ν(CO2) of the dicarbonyl complexes appeared to be between 2063–2088 and 1992–2026 cm^{-1} respectively, while the carbonyl stretching frequency limits for the rhodium(I) monocarbonyl complexes appeared to be between 1960 and 1998 cm^{-1}. The results in Table 1 also indicated that

Table 2
Crystal data and refine parameters for [Rh(acac)(CO)(DPP)].

Identification code	sad
Empirical formula	$RhC_{23}H_{23}NO_3P$
Formula weight	495.805
Temperature	293(2) K
Wavelength	0.71073 Å
Crystal system	Triclinic
Space group	$P\bar{1}$
Unit cell dimensions	a = 10.085(5) Å; b = 12.793(3) Å c = 18.629(5) Å; α = 104.571(5)° β = 100.058(3)°; γ = 106.828(3)°
Volume	2145.6(7) $Å^3$
Z	4
Density (calculated)	1.533 Mg/m^3
Absorption coefficient	0.894 mm^{-1}
F(000)	1008
Crystal size	0.19 × 0.13 × 0.12 mm^3
Theta range for data collection	1.76–28.28°
Index ranges	$-11 \leqslant h \leqslant 13$, $-17 \leqslant k \leqslant 17$, $-20 \leqslant l \leqslant 24$
Reflections collected	14,946
Independent reflections	10,333 [R(int) = 0.0208]
Completeness to theta	97.0%
Absorption correction	None
Refinement method	Full-matrix least-squares on F^2
Data/restraints/parameters	10333/0/526
Goodness-of-fit on F^2	1.013
Final R indices [$I > 2\sigma(I)$]	R_1 = 0.0368, wR_2 = 0.0902
R indices (all data)	R_1 = 0.0571, wR_2 = 0.1009
Largest diff. peak and hole	1.267 and −0.750 e $Å^{-3}$

Table 3
Selected bond lengths (Å) and angles (°) for [Rh(acac)(CO)(DPP)].

Molecule 1		Molecule 2	
Bond	Length (Å)	Bond	Length (Å)
Rh1–C11	1.791(4)	Rh2–C21	1.776(4)
Rh1–O13	2.035(2)	Rh2–O23	2.034(2)
C13–O12	1.280(4)	C23–O11	1.272(4)
Rh1–O12	2.073(2)	Rh2–O22	2.068(2)
Rh1–P1	2.243(1)	Rh2–P2	2.235(1)
P1–C131	1.827(3)	P2–C221	1.825(3)
P1–C111	1.835(3)	P2–C231	1.834(3)
P1–C121	1.832(3)	P2–C211	1.843(3)
N1–C111	1.380(4)	N2–C211	1.362(4)
N1–C115	1.397(5)	N2–C215	1.378(4)
Bond	Angle (°)	Bond	Angle (°)
C11–Rh1–O13	178.52(14)	C21–Rh2–O23	178.37(18)
C11–Rh1–O12	91.75(12)	C21–Rh2–O22	90.16(17)
O13–Rh1–O12	88.16(9)	O23–Rh2–O22	88.54(10)
C11–Rh1–P1	89.62(11)	C21–Rh2–P2	93.23(15)
O13–Rh1–P1	90.56(7)	O23–Rh2–P2	88.10(8)
O12–Rh1–P1	176.40(6)	O22–Rh2–P2	176.14(7)
C131–P1–Rh1	117.99(10)	C221–P2–Rh2	115.46(11)
C111–P1–Rh1	112.85(9)	C231–P2–Rh2	108.65(10)
C121–P1–Rh1	113.77(10)	C211–P2–Rh2	120.42(10)
C13–O12–Rh1	125.6(2)	C23–O22–Rh2	126.0(3)
C15–O13–Rh1	128.1(2)	C26–O23–Rh2	128.0(3)
O11–C11–Rh1	178.0(3)	O21–C21–Rh2	174.8(4)
C131–P1–C111	102.63(13)	C221–P2–C231	105.31(15)
C131–P1–C121	103.71(13)	C221–P2–C211	100.92(14)
C111–P1–C121	104.35(14)	C231–P2–C211	104.62(14)
C111–N1–C115	117.7(3)	C211–N2–C215	117.4(3)
N1–C111–P1	119.8(2)	N2–C211–P2	115.2(2)

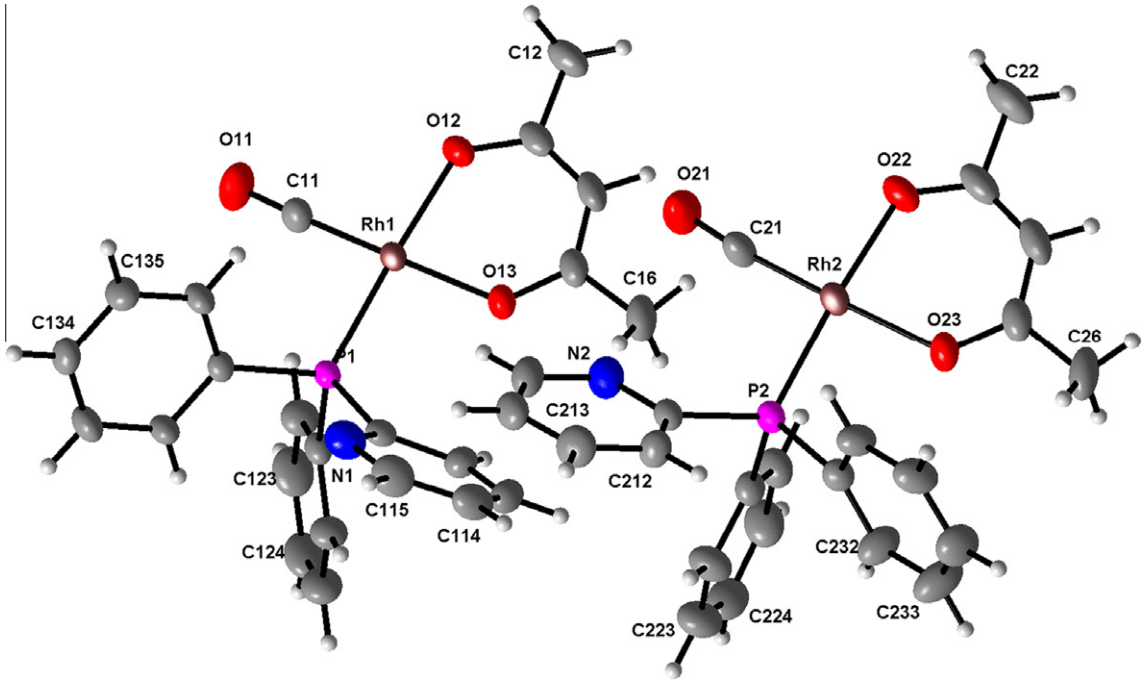

Fig. 2. Numbering scheme of the two different [Rh(acac)(CO)(DPP)] molecules (30% probability displacement ellipsoids).

Table 4
Selected Rh–CO bond distances of [Rh(LL′)(CO)(PX_3)] complexes.

Complex	Rh–CO (Å)	Rh–P (Å)	Refs.
[Rh(cupf)(CO)(PPh_3)]	1.78(1)	2.232(3)	[26,32]
[Rh(acac)(CO)(DPP)]	1.791(4)[a]	2.243(1)[a]	[15,33]
[Rh(neocupf)(CO)(PPh_3)]	1.802(5)	2.227(1)	[32]
[Rh(cupf)(CO){$P(OCH_2)_3CCH_3$}]	1.772(9)	2.156(2)	[26,32]
[Rh(tfdmaa)(CO)(PPh_3)]	1.781(9)	2.239(2)	[11]
[Rh(acac)(CO)(PPh_3)]	1.801(8)	2.244(4)	[24,25]
[Rh(dmavk)(CO)(PPh_3)]	1.784(5)	2.275(1)	[37]
[Rh(fctfa)(CO)(PPh_3)]	1.801(5)	2.232(1)	[44]
[Rh(bap)(CO)(PPh_3)] isomer 1	1.797(4)	2.2376(9)	[45]
[Rh(bap)(CO)(PPh_3)] isomer 2	1.788(5)	2.2387(9)	[45]

[a] This study.

the Rh(III) alkyl and acyl complexes were limited between 2045–2070 and 1692–1721 cm^{-1} respectively. Statistical calculations indicated that interesting predictions could be made from the data in Table 1. These results predicted at a 95% probability [23] that the ν(CO) stretching frequencies for any rhodium(I) dicarbonyl complex would be between 2076 ± 5 ν(CO1) and 2008 ± 5 cm^{-1} ν(CO2) while the stretching frequencies for the rhodium(I) monocarbonyl, rhodium(III) alkyl and acyl complexes would be between 1978 ± 3, 2055 ± 7 cm^{-1} and 1710 ± 6 cm^{-1} respectively if normal distribution was assumed. These results also allowed that the monocarbonyl stretching frequency for newly synthesized rhodium complexes could be approximated according to the following equations:

$$\nu(CO)_{mono} = \nu(CO1) - 100\ cm^{-1} \quad \text{or} \tag{3}$$

$$\nu(CO)_{mono} = \nu(CO2) - 30\ cm^{-1} \tag{4}$$

while the rhodium(III) alkyl and acyl stretching frequency could be approximated according to the following equations:

$$\nu(CO)_{alkyl} = \nu(CO1) - 20\ cm^{-1} \quad \text{or} \tag{5}$$

$$\nu(CO)_{alkyl} = \nu(CO2) + 50\ cm^{-1} \quad \text{or} \tag{6}$$

$$\nu(CO)_{alkyl} = \nu(CO)_{rhodium(I)} + 75\ cm^{-1} \tag{7}$$

and

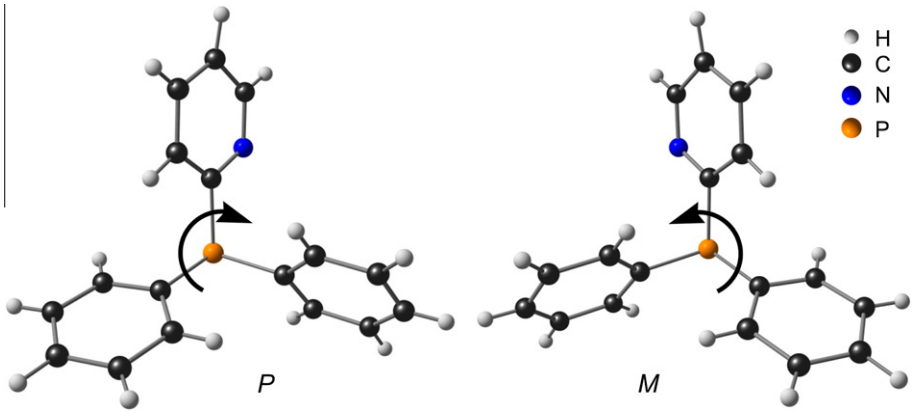

Fig. 3. A representation of free DPP viewed along the σ_{nb}–P axis, demonstrating the enantiomeric configurations *P* (clockwise) and *M* (anti-clockwise).

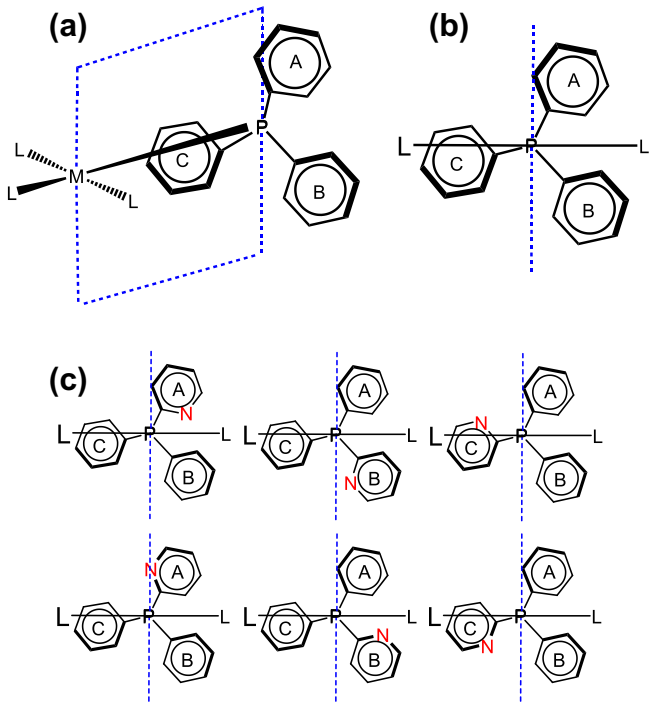

Fig. 4. (a) A projection demonstrating the *plane of nadir energy* (i.e. the plane incorporating all points of minimum steric compression [47], shown by the dotted blue lines) associated with the ligands L attached to a square planar metal center. The predicted minimum energy conformation of PPh_3 in ML_3PPh_3 is also shown. (b) The preferred minimum energy conformation of PPh_3 (as viewed along the P–M bond axis) within square planar [51a] complexes relative to the *plane of nadir energy*. (c) The six possible positions of *N* of pyridyl in DPP all correspond to the same minimum energy conformation of DPP in square planar ML_3DPP. (For interpretation of the references to color in this figure legend, the reader is referred to the web version of this article.)

$$\nu(CO)_{acyl} = \nu(CO1) - 366\ cm^{-1} \quad (8)$$

$$\nu(CO)_{acyl} = \nu(CO)_{rhodium(I)} - 268\ cm^{-1} \quad (9)$$

3.2. Crystal structure

The title complex crystallized in the triclinic space group $P\bar{1}$ with four molecules per unit cell (chloroform as solvent) which is a different for the same complex that crystallized in the monoclinic space group $P2_1/c$ using diethyl ether as solvent [15]. The crystal data for [Rh(acac)(CO)(DPP)] is given in Table 2. The most important bond lengths and angles of the two isomorphic [Rh(acac)(CO)(DPP)] molecules are listed in Table 3 while the numbering scheme is shown in the perspective drawing (Fig. 2). The results clearly showed that the DPP acts a monodentate ligand in both the molecules with the carbonyl ligand bonded *cis* to the phosphine while the rest of the coordination sphere is completed by the two acac oxygen atoms. A comparative study between the two molecules indicated that both adopt a square planar geometry with bond angles varying between 88.10(8)° and 93.23(15)°. The bond distances and angles were of the same magnitude as would be expected for isomorphic systems. The Rh–CO bond length of 1.791 Å for both the mono and triclinic systems correlated well with those found for other [Rh(LL′)(CO)(PX_3)] complexes as can be seen in Table 4. The difference between the two molecules was centered around the orientation of the DPP pyridine ring in the crystal structure. The orientation of the pyridyl nitrogen atom was directed towards the carbonyl ligand in Molecule 2 while the same atom was directed away from the carbonyl group in Molecule 1. This was demonstrated by the intramolecular M–CO···N(pyridyl ring) bond distances of 6.072(2) and 3.290(1) Å as well as the dihedral angles of 61.51(8)° and 47.4(1)° (OCRhP and pyridyl ring as planes) for Molecules 1 and 2 respectively. Closer inspection of the carbon–phosphur–carbon angles in the two molecules also illustrated a smaller bond angle of 100.92(14)° for C221–P2–C211 compared to the rest of the CPC bond angles and correlated well with the identical complex which was isolated from diethyl ether [15]. The pyridyl nitrogen of the phosphine ligand in the monoclinic crystal was also directed more towards the Rh–CO bond, as was the case with Molecule 2 in the current study. The different orientations of the pyridyl group in the three structures, spurred us to undertake a computational chemistry study to determine the preferred conformation (if any) of the DPP group in [Rh(acac)(CO)(DPP)].

3.3. Computational chemistry

The free DPP molecule [46], as well as coordinated DPP can exist in two different helicities, that have the phenyl/pyridyl rings oriented in a clockwise or counter clockwise fashion (referred to as *P* and *M* helicity respectively) similar to PPh_3 [47,48], see Fig. 3. In solution, inversion of the helicity occured readily. In the solid state DPP and PPh_3-containing complexes generally exist as a racemic mixture consisting of units from each helicity in the same unit cell.

Experimental crystal structures [49] and theoretical DFT calculations showed that the lowest energy conformation of PPh_3 coordinated to tetrahedral [47], trigonal-bipyramidal [47], octahedral [50] or square planar metal centers [51] lay in a broad potential energy well having a broad range of energetically acceptable phenyl ring orientations *via* independent P–C_i bond rotations (C_i = C_{ipso} of the phenyl ring Ph). In spite of the wide range of low energy orientations, the orientation of coordinated PPh_3 possessed some distinct features that could be derived from steric principles. Costello [47] has termed the plane incorporating all points of minimum steric compression of a specific complex, the *plane of nadir energy*. The *plane of nadir energy* is illustrated in Fig. 4 for square planar metal centers [51]. The different R substituents on the *P* atom of a tertiary phosphine PR_3 should preferably be oriented as near as possible to the *plane of nadir energy* to have a minimum of steric interaction with the ligands bonded to the complex. In the case of R = Ph the three phenyl rings each will be oriented as near as possible to the *plane of nadir energy*, with a correlated tilting of the phenyl rings (*via* M–P (θ) and P–C_i bond rotations (ω)) in order to minimize both inter ring–ligand and inter ring–ring interactions [51]. The favoured conformation of PPh_3 coordinated to a square planar metal center, illustrated in Fig. 4, can be derived using the following principles [51]: (P helicity, view along P–M axis, C_o = C_{ortho} of the phenyl ring Ph), (i) *superimpose* C_o *of the vertical ring* ***A*** *onto the nadir plane perpendicular to the square plane and allow ring* ***A*** *to tilt towards the smallest ligand, (ii) allow ring* ***B*** *to tilt in the space below the smallest ligand in the quadrant between the nadir plane below the complex and a horizontal plane through the SQP of the complex, (iii) tilt ring* ***C*** *over the largest ligand and (iv) allow correlated tilting of rings* ***A***, ***B*** *and* ***C*** *to minimize inter ring–ring and inter ring–ligand interactions* [51]. We will show that these principles also hold for DPP coordinated to a square planar metal center. PPh_3 (with three Ph groups, each of D_{6h} symmetry) coordinated to a square planar metal center thus having only ONE preferred conformation for *P* helicity (as described above) and ONE preferred conformation for *M* helicity. In contrast, the pyridyl ring in DPP could adopt any of three positions and two orientations for *P* helicity (similar for *M* helicity) that corresponded to the preferred conformation of complex-bound PPh_3. The predicted minimum energy conformation of DPP coordinated to a square planar metal

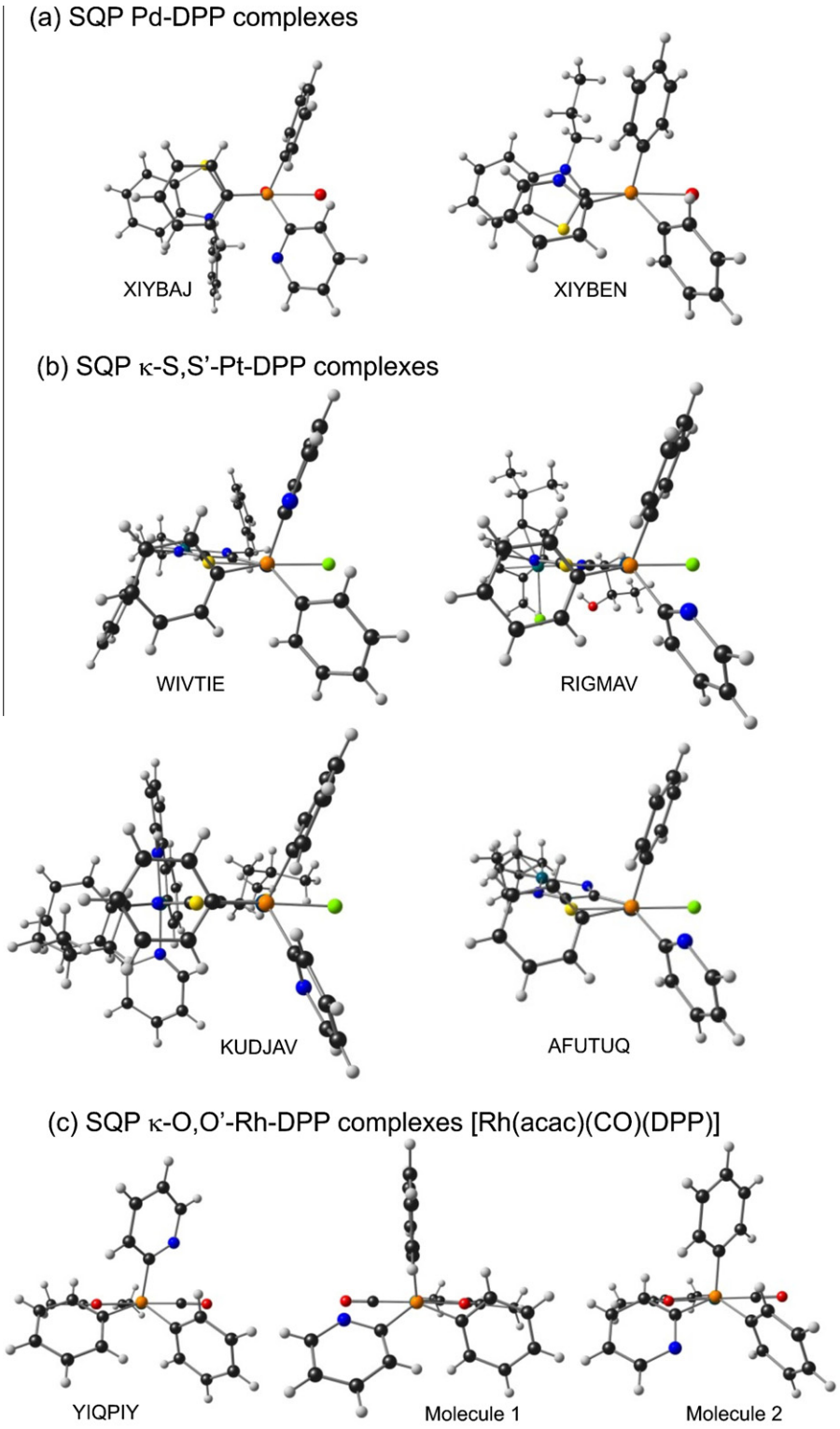

Fig. 5. Geometry of SQP crystals containing on DPP group, as viewed along the P–M axis. CSD reference code shown [49]. For comparative reasons *P* helicities are shown.

center could thus be any of the six illustrated in Fig. 4. We will see that the position of *N* of the pyridyl group in DPP does not have an influence on the minimum energy conformation of DPP.

The orientation of the DPP in selected SQP crystals [49] containing one DPP group is presented in Fig. 5. The orientation of DPP in these experimental crystal structures was similar and is characterized by a near vertical ring **A**, tilted to the right (*P* helicity, except for Molecule 1 of this study) and oriented as near as possible to the *nadir plane* perpendicular to the square plane of the SQP complex, a tilted ring **B** in the quadrant below the square plane and to the right of the *nadir plane* and a near horizontally tilted ring **C** to the left. The orientation of DPP in the structures in Fig. 5a is such that the *vertical ring* **A** is tilted towards the smallest ligand, consistant with the principles for deriving the favoured conformations of

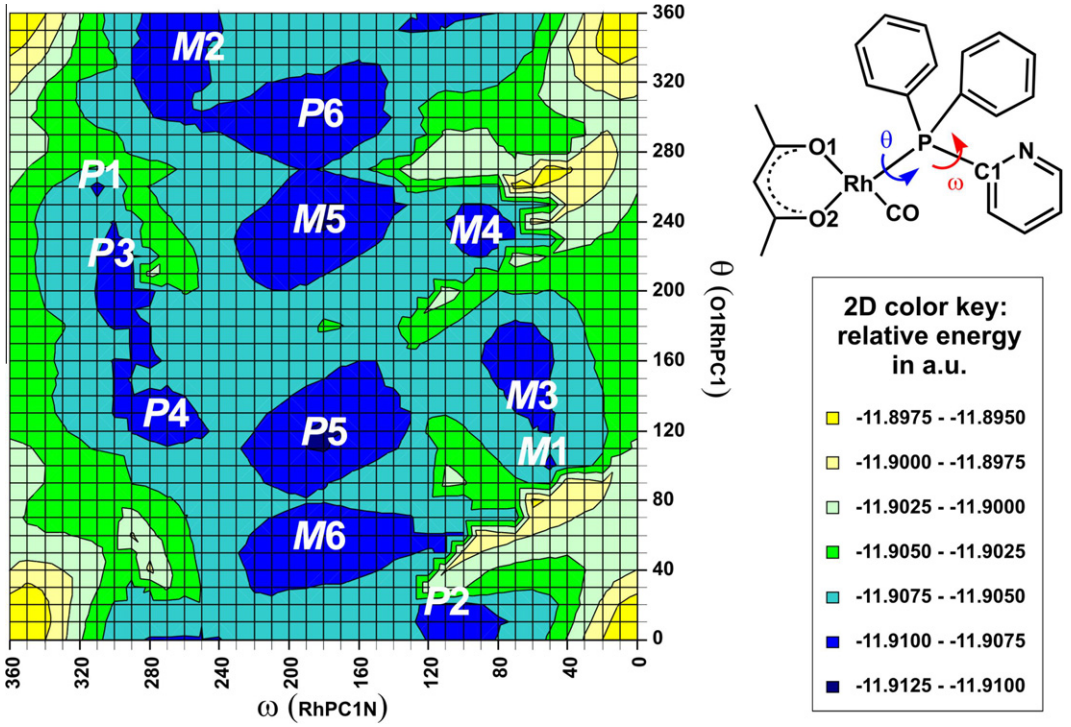

Fig. 6. 2-D potential energy surface (PES) of [Rh(acac)(CO)(DPP)] representing the relative energy of different conformations of DPP in [Rh(acac)(CO)(DPP)] as a function of ω (rotation of a phenyl ring about the P–$C_{pyridyl}$ bond) and θ (rotation of DPP about Rh–P bond). The dark blue areas present the lowest energy geometries (conformations) (1 a.u. = 2625.5 kJ mol^{-1}). The geometry of the complex relating to the minimum energy areas are presented in Fig. 7 according to the numbers indicated. (For interpretation of the references to color in this figure legend, the reader is referred to the web version of this article.)

PPh_3 coordinated to a square planar metal center [51]. We discussed the orientation of DPP here by looking at the steric orientation of the rings without referring to the specific position of *N* of the Py group.

Fig. 6 gives the calculated PES of [Rh(acac)(CO)(DPP)] as a function of dihedral (torsion) angles ω (rotation of the pyridyl ring about the P–C_{Ph} bond) and θ (rotation of DPP about the Rh–P bond). The PES is obtained by rotation of the DPP group through 360° and

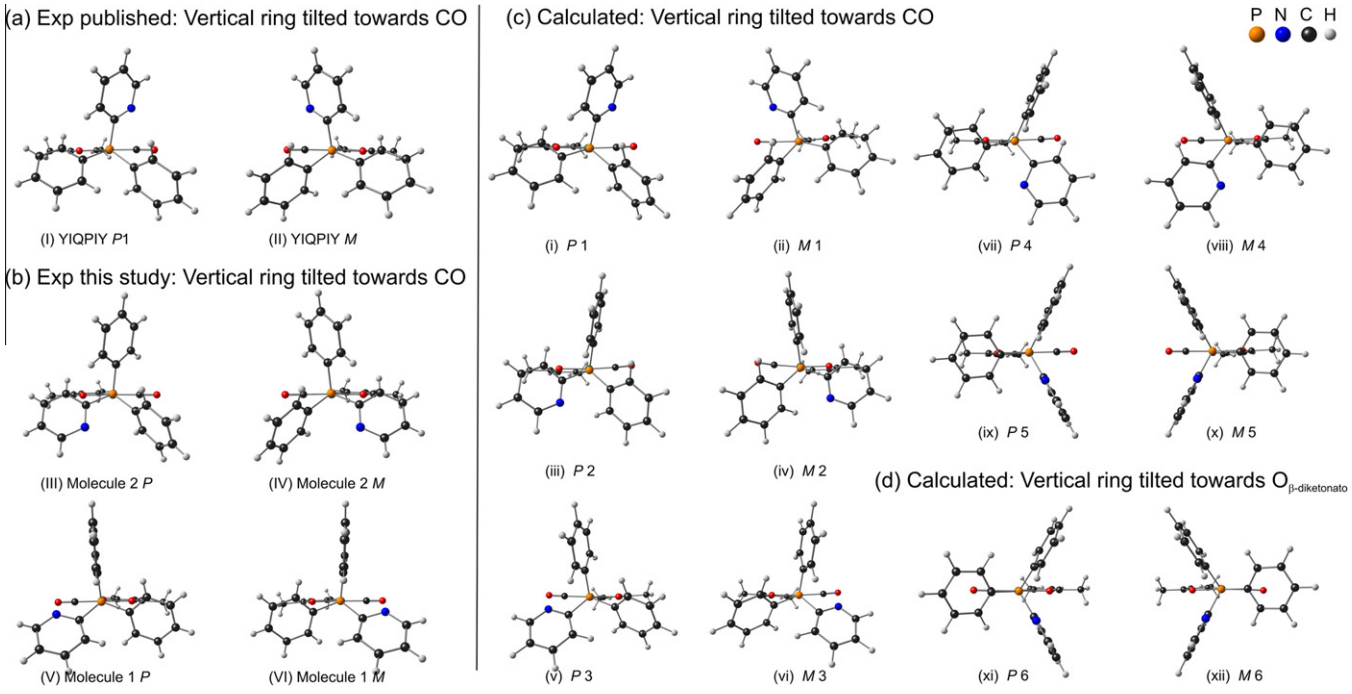

Fig. 7. The experimental (I–VI) and the DFT calculated minimum energy conformations (i–xii) of [Rh(acac)(CO)(DPP)] as viewed along the P–Rh axis. In (a–c) the vertical phenyl ring is tilted towards CO and in (d) the vertical phenyl ring is tilted towards $O_{\beta\text{-diketonato}}$. The numbering of the calculated structures corresponds to the numbering of the minimum energy areas of the PES in Fig. 6.

the simultaneous rotation of the pyridyl ring from 0° to 360° at each point, resulting in 1296 restrained optimizations. Every point on the graph thus presents a conformation of [Rh(acac)(CO)(DPP)] with two dihedrals related to the pyridyl ring restricted and the rest of the molecule fully optimized. The other two phenyl rings were thus free to rotate in order to minimize steric interaction towards a lower electronic energy geometry. The PES results in 12 areas of minimum energy. Careful examination of the geometries of these 12 minimum energy structures resulted in six different conformations with *P* helicity and their enantiomers (mirror images) as displayed in Fig. 7c and d. The 12 enantiomers are near equi-energetic.

The orientation of the DPP group in the conformations in Fig. 7(i and ii) were similar to the previously published crystal structure of [Rh(acac)(CO)(DPP)] (CSD code YIQPIY) [15]. The four conformations Fig. 7(iii–vi) are similar to the Molecule 1 and Molecule 2 of the crystal structure of [Rh(acac)(CO)(DPP)] presented in this study. The only difference was that the vertical ring in the experimental structures is orientated slightly differently, probably due to packing effects. The other six minimum energy conformations have one (Fig. 7(vii–viii)) or two (vii–xii) rings near perpendicular to the paper, orientations not experimentally observed for [Rh(acac)(CO)(DPP)] complexes. However, we observe that the orientation of DPP in Fig. 7(x–xii) correspond to the orientation of DPP in the SQP -S,S′-Pt-DPP complex with crystal code KUDJAV in Fig. 5b. The experimental and DFT calculated results did not show any preference for the position of *N* (illustrated in Fig. 4) of the pyridyl group in the minimum energy orientation of complex-bound DPP.

4. Conclusion

The crystal structure of [Rh(acac)(CO)(DPP)] clearly showed that the DPP acts a monodentate ligand in the structurally characterized compounds. [Rh(acac)(CO)(DPP)] crystallized in the triclinic space group $P\bar{1}$ with four molecules per unit cell, contrary to previously published work where [Rh(acac)(CO)(DPP)] crystallized in the monoclinic space group [15]. The conformation analysis of DPP coordinated to [Rh(acac)(CO)(DPP)] resulted in 12 areas of minimum energy, most lying in a broad energy well of low energy orientations. The conformation of four of the 12 areas of minimum energy agreed with the crystal structures of the *P* and *M* helicities of Molecules 1 and 2 of [Rh(acac)(CO)(DPP)] presented in this study. DFT calculations also confirmed the experimental observations that more than one preferred *N* position of the pyridyl group exists for the complex-bound DPP in these type of complexes.

Supplementary data

CCDC No. 770106 contains the supplementary crystallographic data for this paper.

Acknowledgements

The authors thank the Research Fund of the University of the Free State, the National Research Fund of the Republic of South Africa and Dr. L. Twigge for her contribution to the NMR interpretations.

References

[1] W.A. Herrmann, B. Cornils, Applied Homogeneous Catalysis with Organometallic Compounds, VCH Weinheim, 1999.
[2] G.W. Parshall, S.D. Ittel, Homogeneous Catalysis, second ed., Wiley-Interscience, New York, 1992. p. 96.
[3] K. Weissermel, H.J. Arpe, Industrial Organic Chemistry, third ed., VCH, Weinheim, 1997.
[4] H.M. Colquhoun, D.J. Thompson, M.V. Twigg, Carbonylation: Direct Synthesis of Carbonyl Compounds, Plenum Press, New York, 1991.
[5] A. Haynes, P.M. Maitlis, G.E. Morris, G.J. Sunley, H. Adams, P.W. Badger, C.M. Bowers, B. Cook, P.I.P. Elliot, T. Ghaffar, H. Green, T.R. Griffin, M. Payne, J.-M. Pearson, M.J. Taylor, P.W. Vickers, R.J. Watt, J. Am. Chem. Soc. 126 (2004) 2847.
[6] T.W. Dekleva, D. Foster, Adv. Catal. 34 (1986) 81.
[7] H. Kidwell, January 2008. <www.in-pharmatechnologist.com/content/> (accessed 16.03.10).
[8] R.A. Howard, T.G. Spring, J.L. Bear, Cancer Res. 36 (1976) 4402.
[9] H.T. Chifotides, K.R. Dunbar, Acc. Chem. Res. 38 (2005) 146.
[10] D. Forster, J. Am. Chem. Soc. 98 (1976) 846.
[11] (a) S.S. Basson, J.G. Leipoldt, J.T. Nel, Inorg. Chim. Acta 86 (1984) 167;
(b) S.S. Basson, J.G. Leipoldt, A. Roodt, J.A. Venter, T.J. van der Walt, Inorg. Chim. Acta 119 (1986) 35;
(c) S.S. Basson, J.G. Leipoldt, A. Roodt, J.A. Venter, Inorg. Chim. Acta 128 (1987) 31;
(d) J.G. Leipoldt, S.S. Basson, L.J. Botha, Inorg. Chim. Acta 168 (1990) 215;
(e) J.G. Leipoldt, E.C. Steynberg, R. van Eldik, Inorg. Chem. 26 (1987) 3068;
(f) G.J. van Zyl, G.J. Lamprecht, J.G. Leipoldt, T.W. Swaddle, Inorg. Chim. Acta 143 (1988) 223;
(g) J.G. Leipoldt, G.J. Lamprecht, G.J. van Zyl, Inorg. Chim. Acta 96 (1985) L31;
(h) D.M.C. Smit, S.S. Basson, A. Roodt, E.C. Steynberg, Rhodium Express 7–8 (1994) 12;
(i) Y.M. Terblans, S.S. Basson, W. Purcell, G.J. Lamprecht, Acta Cryst. C51 (1995) 1748;
(j) P. Ebenebe, S.S. Basson, W. Purcell, Rhodium Express 16 (1996) 11;
(k) M. Theron, E. Grobbelaar, W. Purcell, S.S. Basson, Inorg. Chim. Acta 358 (2005) 2457;
(l) E. Grobbelaar, W. Purcell, S.S. Basson, Inorg. Chim. Acta 359 (2006) 3800;
(m) J. Conradie, G.J. Lamprecht, A. Roodt, J.C. Swarts, Polyhedron 23 (2007) 5075;
(n) M.M. Conradie, J. Conradie, Inorg. Chim. Acta 361 (2008) 2285;
(o) J. Conradie, J.C. Swarts, Organometallics 28 (2009) 1018;
(p) A.J. Muller, J. Conradie, W. Purcell, S.S. Basson, J.A. Venter, S. Afr, J. Chem. 63 (2010) 11;
(q) M.M. Conradie, J. Conradie, Dalton Trans. 40 (2011) 8226;
(r) K.H. Hopmann, J. Conradie, Organometallics 28 (2009) 3710.
[12] (a) K. Wajda-Hermanowicz, Z. Ciunik, A. Kochel, Inorg. Chem. 45 (2006) 3369;
(b) K. Wajda-Hermanowicz, F.P. Pruchnik, Trans. Met. Chem. 13 (1988) 22.
[13] (a) N.W. Alcock, P. Moore, P.A. Lampe, K.F. Mock, J. Chem. Soc. Dalton Trans. (1982) 207;
(b) M.M. Olmstead, A. Maisonnat, J.P. Farr, A.L. Balch, Inorg. Chem. 20 (1981) 4060;
(c) Y. Inoguchi, B. Milewski-Marla, H. Schmidbauer, Chem. Berichte 115 (1982) 3085;
(d) H.J. Wasserman, D.C. Moody, R.T. Paine, R.R. Ryan, K.V. Salazar, J. Chem. Soc. Chem. Commun. (1984) 533.
[14] (a) U. Abrama, R. Albertob, J.R. Dilworthc, Y. Zhengc, K. Ortne, Polyhedron 18 (1999) 2995;
(b) P. Govindaswamy, P.J. Carroll, Y. Mozharivskyj, M.R. Kollipara, J. Chem. Sci. 118 (2006) 319;
(c) J.-L. Zhou, Y.-Z. Li, H.-G. Zheng, X.-Q. Xinand, L.-L. Xu, Acta Cryst. E59 (2003) m176.
[15] M. Coetzee, W. Purcell, H.G. Visser, J.A. Venter, Acta Cryst. E63 (2007) m3165.
[16] T.T. Chiweshe, W. Purcell, J.A. Venter, S. Afr, J. Chem. 66 (2012) 7.
[17] Bruker SAINT-Plus (version 7.12) and SADABS (version 2004/1), Bruker AXS Inc., Madison, Wisconsin, USA, 2004.
[18] G.M. Sheldrick, SHELXL97, University of Göttingen, Göttingen, Germany, 1997.
[19] A.L. Spek, PLATON(C), Utrecht University, Utrecht, the Netherlands, 1980–2011.
[20] K. Goswami, M.M. Singh, Trans. Met. Chem. 5 (1980) 83.
[21] (a) ADF 2012.01, SCM, Theoretical Chemistry, Vrije Universiteit Amsterdam, Amsterdam, the Netherlands.;
(b) G. te Velde, F.M. Bickelhaupt, E.J. Baerends, C. Fonseca Guerra, S.J.A. van Gisbergen, J.G. Snijders, T. Ziegler, J. Comput. Chem. 22 (2001) 931;
(c) C. Fonseca Guerra, J.G. Snijders, G. te Velde, E.J. Baerends, Theor. Chem. Acc. 99 (1998) 391.
[22] (a) J.P. Perdew, J.A. Chevary, S.H. Vosko, K.A. Jackson, M.R. Pederson, D.J. Singh, C. Fiolhais, Phys. Rev. B 46 (1992) 6671;
. Erratum:(b) J.P. Perdew, J.A. Chevary, S.H. Vosko, K.A. Jackson, M.R. Pederson, D.J. Singh, C. Fiolhais, Phys. Rev. B 48 (1993) 4978.
[23] D.A. Skoog, D.W. West, F.J. Holler, S.R. Crouch, Fundamentals of Analytical Chemistry, 8th ed., Thomson – Brook/Cole, Australia, 2004.
[24] F. Bonati, G. Wilkinson, J. Chem. Soc. (1964) 3156.
[25] J.G. Leipoldt, S.S. Basson, L.D.C. Bok, T.I.A. Gerber, Inorg. Chim. Acta 26 (1978) L35.
[26] S.S. Basson, J.G. Leipoldt, A. Roodt, J.A. Venter, Inorg. Chim. Acta 118 (1986) L45.
[27] W. Chen, Y. Xu, S. Liao, Trans. Met. Chem. 19 (1994) 418.
[28] P.N. Ebenebe, A mechanistic and structural study of carbonyl substitution in square-planar rhodium(I)-beta-diketone complexes, M.Sc. Thesis, UFS, Bloemfontein, South Africa, 1998.
[29] J.G. Leipoldt, L.D.C. Bok, S.S. Basson, J.S. van Vollenhoven, T.I.A. Gerber, Inorg. Chim. Acta 25 (1977) L634.
[30] J. Conradie, G.J. Lamprecht, S. Otto, J.C. Swarts, Inorg. Chim. Acta 328 (2002) 191.

[31] N.F. Stuurman, R. Meijboom, J. Conradie, Polyhedron 30 (2011) 660.
[32] J.A. Venter, Structural and kinetic study of rhodium complexes of N-aryl-N-nitrosohydroxylamines and related complexes, Ph.D. Thesis, UFS, Bloemfontein, South Africa, 2006.
[33] M.P. Coetzee, Characterization and oxidative addition reactions of different rhodium(I) carbonyl diphenyl-2-pyridylphosphine complexes, M.Sc. Thesis, UFS, Bloemfontein, South Africa, 2008.
[34] L.J. Damoense, W. Purcell, A. Roodt, J.G. Leipoldt, Rhodium Express 5 (1994) 10.
[35] M.M. Conradie, J. Conradie, Inorg. Chim. Acta 361 (2008) 208.
[36] N.F. Stuurman, J. Conradie, J. Organomet. Chem. 694 (2009) 259.
[37] L.J. Damoense, W. Purcell, A. Roodt, J.G. Leipoldt, Rhodium Express 14 (1995) 4.
[38] G.J.J. Steyn, Organometallic rhodium(I) chemistry, Ph.D. Thesis, UFS, Bloemfontein, South Africa, 1995.
[39] G.J.J. Steyn, A. Roodt, J.G. Leipoldt, Rhodium Express (1993) 11.
[40] M.A. Bennett, J.C. Jeffery, G.B. Robertson, Inorg. Chem. 20 (1981) 323.
[41] H. Adams, N.A. Bailey, B.E. Mann, C.P. Manuel, Inorg. Chim. Acta 198 (1992) 111.
[42] L. Gonsalvi, H. Adams, G.J. Sunley, E. Ditzel, A. Haynes, J. Am. Chem. Soc. 124 (2002) 13597.
[43] K.G. Moloy, J.L. Petersen, Organometallics 14 (1995) 2931.
[44] G.J. Lamprecht, J.C. Swarts, J. Conradie, J.G. Leipoldt, Acta Cryst. CA9 (1993) 82.
[45] K.H. Hopmann, N.F. Stuurman, A. Muller, J. Conradie, Organometallics 29 (2010) 2446.
[46] J.-P. Charland, J.-L. Roustan, N. Ansari, Acta Cryst. C45 (1989) 680.
[47] J.F. Costello, S.G. Davies, J. Chem. Soc. Perkin Trans. 2 (1998) 1683.
[48] À. Pintèr, G. Haberhauer, I. Hyla-Kryspin, S. Grimme, Chem. Commun. (2007) 3711.
[49] Cambridge Structural Database (CSD), Version 5.33, February 2012.
[50] J.F. Costello, S.G. Davies, D. McNally, J. Chem. Soc. Perkin Trans. 2 (1999) 465.
[51] (a) J. Conradie, Dalton Trans. 41 (2012) 10633;
(b) N.F. Stuurman, A. Muller, J. Conradie, Inorg. Chim. Acta 395 (2013) 237;
(c) N.F. Stuurman, A. Muller, J. Conradie, Trans. Met. Chem. (2013) submitted for publication.